Agricultural and Forest Meteorology 249 (2018) 367–376

Contents lists available at ScienceDirect

Agricultural and Forest Meteorology

journal homepage: www.elsevier.com/locate/agrformet

The role of surface roughness, albedo, and Bowen ratio on ecosystem energy balance in the Eastern United States

Elizabeth Burakowski[a,b,*], Ahmed Tawfik[a], Andrew Ouimette[b], Lucie Lepine[b,c], Kimberly Novick[d], Scott Ollinger[b], Colin Zarzycki[a], Gordon Bonan[a]

[a] Climate and Global Dynamics Division, National Center for Atmospheric Research, 300 Table Mesa Drive, Boulder, CO 03805, United States
[b] Institute for the Study of Earth, Oceans,and Space, University of New Hampshire, 8 College Road, Durham, NH 03824, United States
[c] United States Department of Agriculture Forest Service, Northern Research Station, 271 Mast Road, Durham, NH 03824, United States
[d] School of Public and Environmental Affairs, Indiana University, 1315 E 10th Street, Bloomington, IN 47405, United States

ARTICLE INFO

Keywords:
Land cover and land use change
Albedo
Surface roughness
Evapotranspiration
Earth system models
Eddy covariance

ABSTRACT

Land cover and land use influence surface climate through differences in biophysical surface properties, including partitioning of sensible and latent heat (e.g., Bowen ratio), surface roughness, and albedo. Clusters of closely spaced eddy covariance towers (e.g., < 10 km) over a variety of land cover and land use types provide a unique opportunity to study the local effects of land cover and land use on surface temperature. We assess contributions albedo, energy redistribution due to differences in surface roughness and energy redistribution due to differences in the Bowen ratio using two eddy covariance tower clusters and the coupled (land-atmosphere) Variable-Resolution Community Earth System Model. Results suggest that surface roughness is the dominant biophysical factor contributing to differences in surface temperature between forested and deforested lands. Surface temperature of open land is cooler (−4.8 °C to −0.05 °C) than forest at night and warmer (+0.16 °C to +8.2 °C) during the day at northern and southern tower clusters throughout the year, consistent with modeled calculations. At annual timescales, the biophysical contributions of albedo and Bowen ratio have a negligible impact on surface temperature, however the higher albedo of snow-covered open land compared to forest leads to cooler winter surface temperatures over open lands (−0.4 °C to −0.8 °C). In both the models and observation, the difference in mid-day surface temperature calculated from the sum of the individual biophysical factors is greater than the difference in surface temperature calculated from radiative temperature and potential temperature. Differences in measured and modeled air temperature at the blending height, assumptions about independence of biophysical factors, and model biases in surface energy fluxes may contribute to daytime biases.

1. Introduction

Land cover influences surface climate through radiative (i.e. albedo) and non-radiative (i.e. surface roughness and Bowen ratio) biophysical surface properties (Bonan, 2008). Non-forested land generally has a higher albedo than forested land (Betts and Ball, 1997; Moody et al., 2007; Jin et al.,2002), which leads to daytime cooling in deforested areas. The surface roughness warms forest relative to open land by drawing warmer air from aloft via increased turbulence at night; during the day, deforested lands experience suppressed mixing while forests cool through more efficient dissipation of sensible heat (Rotenberg and Yakir, 2010). At night, surface roughness cools open land relative to forests, which are hypothesized to draw warmer air from aloft through increased turbulent mixing and release a greater amount of stored heat compared to open lands (Lee et al., 2011; Schultz et al., 2017). During the growing season, forests often have cooler surface temperatures than open fields due to greater evaporative cooling (i.e. higher Bowen ratio; Juang et al., 2007). However, irrigation of cropland can increase the Bowen ratio and cool surface temperatures over open lands compared to forests (Adegoke et al., 2003; Kueppers et al., 2007).

In addition to the general biophysical responses across land cover types, the relative contributions of albedo, Bowen ratio, and roughness to differences in surface temperature can vary by biome and latitude. In the high latitudes, albedo has been recognized as the dominant biophysical forcing factor of land cover on surface climate, primarily due to snow cover (Feddema et al., 2005; Betts et al., 2007; Davin et al., 2007; Burakowski et al., 2016). In the tropics, forests cool surface temperatures through enhanced evapotranspiration compared to

* Corresponding author. Institute for the Study of Earth, Oceans, and Space, University of New Hampshire, 8 College Road, Durham, NH 03824, United States.
E-mail addresses: elizabeth.burakowski@unh.edu (E. Burakowski), abtawfik@ucar.edu (A. Tawfik), andrew.ouimette@unh.edu (A. Ouimette), lucie.lepine@unh.edu (L. Lepine), knovick@indiana.edu (K. Novick), scott.ollinger@unh.edu (S. Ollinger), zarzycki@ucar.edu (C. Zarzycki), bonan@ucar.edu (G. Bonan).

https://doi.org/10.1016/j.agrformet.2017.11.030
Received 9 June 2017; Received in revised form 25 October 2017; Accepted 26 November 2017
Available online 02 December 2017

grassland and cropland (Li et al., 2015). In the mid-latitudes, however, the contribution of LULCC-driven differences in albedo, evapotranspiration, and surface roughness to biophysical forcing of surface climate remains unclear (Bonan 2008).

Multiple global climate model studies have concluded that historical mid-latitude deforestation cooled the Northern Hemisphere, primarily through an increase in surface albedo when agricultural lands replaced forest (Brovkin et al., 2006; Betts, 2001; Betts et al., 2007; Davin and de Noblet-Ducoudré, 2010; Kvalevåg et al., 2010). The presence of seasonal snow cover in the mid-latitudes strengthens cooling over open lands relative to forest due to the increased surface albedo over open lands resulting from snow burial of the short canopy.

Non-radiative processes such as evaporative efficiency and surface roughness have recently been acknowledged as having an effect on surface temperature comparable in magnitude and opposite in sign to radiative processes. Davin and de Noblet-Ducoudré (2010) conducted a series of idealized global deforestation experiments with the Institut Pierre-Simon Laplace (IPSL) model to evaluate the relative contributions of albedo, surface roughness, and evapotranspiration efficiency on surface temperature differences between forest and grassland. Between 40°N and 50°N, radiative cooling of grasslands compared to forests from albedo (−2.2 K) was mitigated by warming from non-radiative surface roughness (+1.1 K) and evapotranspiration efficiency (+0.75 K) effects. Nonlinear effects were calculated as the residual between the reconstructed signal and overall net biogeophysical effect, however the mechanisms explaining possible nonlinear interactions were not explored. Using the Community Climate System Model (CCSM), Lawrence and Chase (2010) report that reductions in evapotranspiration and latent heat are the primary drivers of surface temperature changes resulting from land cover change, with radiative forcing playing a secondary role. A similar finding was reported in the 'Land-Use and Climate, Identification of robust impacts' (LUCID) multi-model ensemble of global climate models (de Noblet-Ducoudré et al., 2012). A multi-variate analysis demonstrated that surface cooling from historical deforestation is significantly dampened by non-radiative processes (Boisier et al., 2012).

Studies that used remote sensing approaches also highlight the importance of non-radiative processes on surface temperature. For example, using satellite-derived albedo, land surface temperature (LST), and evapotranspiration (ET), Zhao and Jackson (2014) evaluated the biophysical effects of LULCC on LST. They found that longwave radiative forcing induced by changes in LST and ET were comparable or exceeded the shortwave radiative forcing from changes in albedo (Zhao and Jackson, 2014). Li et al. (2015) suggest that between 35°N and 45°N, the biophysical effects of albedo (i.e., cooling) and evapotranspiration (i.e., warming) are equivalent and opposite in sign, leading to weak differences in land surface temperature between forested and deforested lands. An analysis that combined ground observations and remote sensing demonstrated that surface cooling from increased albedo of deforested lands is offset by warming from decreased sensible heat fluxes, resulting in a net warming at the surface (Luyssaert et al., 2014). Most recently, Bright et al. (2017) combined remote sensing and in situ observations to demonstrate that non-radiative processes dominate local responses to land cover and land management changes.

Observations from eddy covariance towers suggest that the overall cooling effect from deforestation is strongly influenced by non-radiative processes. In the southeastern United States, the effects of eco-physiological and aerodynamic attributes cooled hardwood and pine forests relative to grassland by 2.9 °C and 2.1 °C, respectively, compared to albedo, which warmed forests by 0.7 °C to 0.9 °C (Juang et al., 2007). In California, an oak savanna daily-averaged potential air temperature was 0.5 °C warmer than an adjacent annual grassland due to the lower albedo and aerodynamic roughness (Baldocchi and Ma, 2013). Lee et al. (2011) formulated the intrinsic biophysical mechanism to decompose the factors contributing to surface temperature differences between forested and open lands. Specifically, an observed surface temperature difference can be separated into the energy exchange due to differences in albedo, surface roughness, and Bowen ratio. In temperate regions, the low surface roughness of non-irrigated grasslands contributes 1 K of annual surface temperature warming relative to forests. In contrast, higher surface albedo of grasslands cools surface temperature by −0.5 K and increased Bowen ratio also cools grasslands by −0.25 K (Lee et al., 2011). However, a diurnal asymmetry leads to a stronger surface roughness effect during the day (+2 K warming over grasslands) than at night (−0.5 K cooling over grasslands). During the daytime, the increased surface roughness of forest canopies contributes to greater dissipation of heat compared to aerodynamically smooth grasslands, whereas the mixing at night above forests canopies draws warmer air from aloft (Schultz et al., 2017). A similar paired FLUXNET site study confirmed surface roughness as the dominant biogeophysical feedback from land cover and land use change, however coupled climate model deforestation experiments indicated that large scale atmospheric changes, or indirect feedbacks, tend to mitigate the direct effect of surface roughness (Chen and Dirmeyer, 2016).

Here, we build upon previous modeling and observational eddy covariance studies to evaluate how well a coupled land-atmosphere model simulates biophysical contributions of albedo, surface roughness, and evapotranspiration to surface temperature in a mid-latitude temperate region of the Eastern United States. We compare sub-grid simulations performed using the Variable-Resolution Community Earth System Model (VR-CESM) to two eddy covariance tower clusters in the Eastern United States. The eastern United States was chosen because of the availability of two closely spaced tower clusters that represent dominate forest and deforested land cover types in the region. Observational towers located within close proximity receive more similar atmospheric forcing conditions than towers located tens or hundreds of kilometers apart. The close proximity thus more closely resembles conditions simulated for sub-grid model output, in which plant functional types receive the same atmospheric forcing conditions for a given grid cell. First, we evaluate tower-derived and modeled contributions of albedo, roughness, and evaporative cooling using the Lee et al. (2011) approach at the site level. We then use sub-grid, PTF-level regional simulations to explore spatial differences in biophysical factors over the entire eastern US.

2. Datasets and methods

2.1. Eddy covariance tower clusters

2.1.1. University of New Hampshire, Durham, New Hampshire (NH)

The tower cluster in Durham, New Hampshire was installed in 2014 and includes three Eddy covariance towers that collect data over a cornfield (UNH-corn), a hayfield consisting of C3 non-arctic grass (UNH-grass), and a broadleaf deciduous temperate forest (UNH-hardwood) (Fig. 1). The sampling period included uninterrupted snow cover from January 2015 through late March 2015 at all three sites, with snow cover persisting through early April 2015 at the UNH-hardwood site.

The towers sampled meteorological and near-surface eddy covariance fluxes at half-hourly intervals (Table 1). Turbulent sensible and latent heat fluxes were measured using a LI-COR® LI-7200 enclosed path CO_2/H_2O analyzer and Gill® Windmaster sonic anemometer at 1 m above the cornfield and hayfield canopies, and 5 m above the forest canopy. Turbulent fluxes were calculated using the EddyPro® open source software (EddyPro®, 2014). Radiative fluxes were measured using Kipp & Zonen CNR4 net radiometers that measure incoming and outgoing longwave and shortwave radiation at each tower.

Gap filling for missing meteorological data (air temperature, incoming shortwave, precipitation, relative humidity, and wind speed) in the flux tower cluster was performed using two United States Climate Reference Network (USCRN) stations that provide sub-hourly

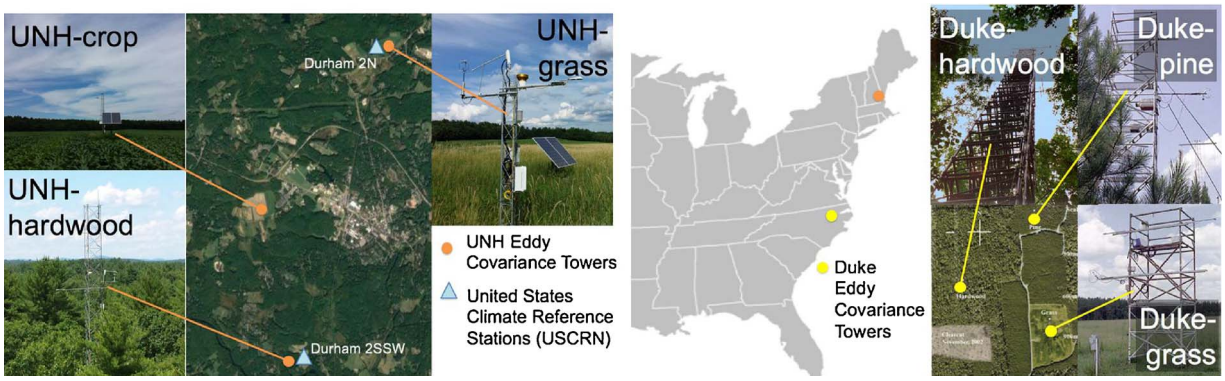

Fig. 1. Eddy covariance tower clusters in the Eastern US. Durham, NH sites include UNH-grass, UNH-hardwood and UNH-crop, and two United States Climate Reference Network (USCRN) stations. Durham, NC sites include Duke-grass, Duke-hardwood, and Duke-pine.

meteorological data, available from 2002 to present. The USCRN Durham 2N station is located 400 m west of the UNH-grass tower; the USCRN Durham 2SSW is located in a hayfield 400 m east of the UNH-hardwood tower (Fig. 1). Meteorological data from the Durham 2N station were used to fill missing meteorological data in the UNH-grass tower and the UNH-crop tower. Missing data from the UNH-hardwood tower was filled using meteorological data from the Durham 2SSW tower.

Any remaining missing data in the flux tower record (< 0.01% of the half-hourly data) were filled using linear interpolation. Filled meteorological variables include air temperature (T_a), relative humidity (*RH*), precipitation (*PRCP*), incoming shortwave radiation (SW_{in}), and wind speed (*WS*). Missing pressure data in the flux towers were filled using the National Weather Service Automatic Surface Observing System (NWS/ASOS) data collected at Portsmouth International Airport at Pease in Portsmouth, NH (PSM). The amount of missing data gap-filled with USCRN data varied by site and by variable. At a maximum, no more than 26% of meteorological data were gap-filled at UNH-grass, less than 20% at UNH-corn, and less than 5% at UNH-hardwood. Details on data processing and gapfilling are detailed in Burakowski et al. (in review).

2.1.2. Duke Forest, Durham, North Carolina (NC)

The Duke Forest tower cluster includes three ecosystems: an open field dominated by a C3 non-arctic grass (*Alta fescue;* Duke-grass), a broadleaf deciduous temperate hardwood forest (Duke-hardwood), and a needleleaf evergreen temperate forest composed of Loblolly Pine (Duke-Pine) (Fig. 1). We included meteorological and surface energy flux data collected between 2004 and 2008. Details on quality control and gapfilling of the Duke Forest tower sites are described in Novick et al. (2009, 2015) and Burakowski et al. (in review).

2.2. Variable-Resolution Community Earth System Model (VR-CESM1.3)

The impacts of land-atmosphere coupling on biophysical forcings of land cover and land use are explored using the Variable-Resolution-Community Earth System Model, version 1.3 (VR-CESM1.3; Zarzycki et al., 2015), which includes the Community Atmosphere Model, version 5.3 (CAM5.3; Neale et al., 2010) and CLM4.5 (Oleson et al., 2013). The Community Earth System Model (CESM) is a state-of-the-art global climate model jointly developed by the National Center for Atmospheric Research (NCAR) and the Department of Energy (DOE). Variable-Resolution (VR-CESM) capabilities have been recently implemented in the CESM framework. VR-CESM allows for a reduction in computational cost by regionally targeting areas requiring higher spatial resolution without adversely impacting the global circulation (Zarzycki et al., 2014, 2015). The VR-CESM1.3 simulations were run with a 1° (~111 km) global grid that contained a 0.25° (~28 km) area of regional refinement over the eastern United States (Fig. 2). The simulations ran from 1979–2008 using prescribed historical sea surface temperatures and sea ice and a 50-year spin-up period for CLM4.5 (Oleson et al., 2013). The CESM configuration used here follows Atmospheric Intercomparison Project (AMIP) protocols (Gates 1992).

To fully take advantage of the VR-CESM coupled simulations, data were output at the sub-grid plant functional type (PFT) level and a temporal frequency of 3-h. Outputting at the PFT-level accomplished two goals. First, we can perform one-to-one comparison against flux tower sites of a similar PFT category, thus avoiding the issue of grid cell averaged state and flux variables across multiple PFTs, as is typically done in coupled model simulations. Second, we uphold a primary assumption of the intrinsic biophysical mechanism decomposition (Lee et al., 2011) that states air must be sufficiently blended between the forested and open sites such that they experience the same forcing temperature. This is exactly what occurs in the VR-CESM simulations

Table 1
Eddy covariance flux tower clusters and Plant Function Types (PFT) used in CLM.

Site ID	Simulation period	Lat (N)	Lon(W)	Elevation (m)	Tower Height (m)	PFT
UNH, Durham, NH	2014–2015					
UNH-grass		43.1717	−70.9259	33	3.6	C3NAG[a]
UNH-crop		43.1385	−70.9610	20	3.0	CRO[b]
UNH-hardwood		43.1085	−70.9522	40	30	BDT[c]
Duke, Durham, NC	2004–2008					
Duke-grass		35.9712	−79.0934	168	2.8	C3NAG[a]
Duke-hardwood		35.9736	−79.1004	168	39.8	BDT[c]
Duke-pine		35.9782	−79.0942	168	20.2	NET[d]

[a] C3 Non-Arctic Grass.
[b] Crop (e.g., corn).
[c] Broadleaf Deciduous Temperate Forest.
[d] Needleleaf Evergreen Temperate Forest.

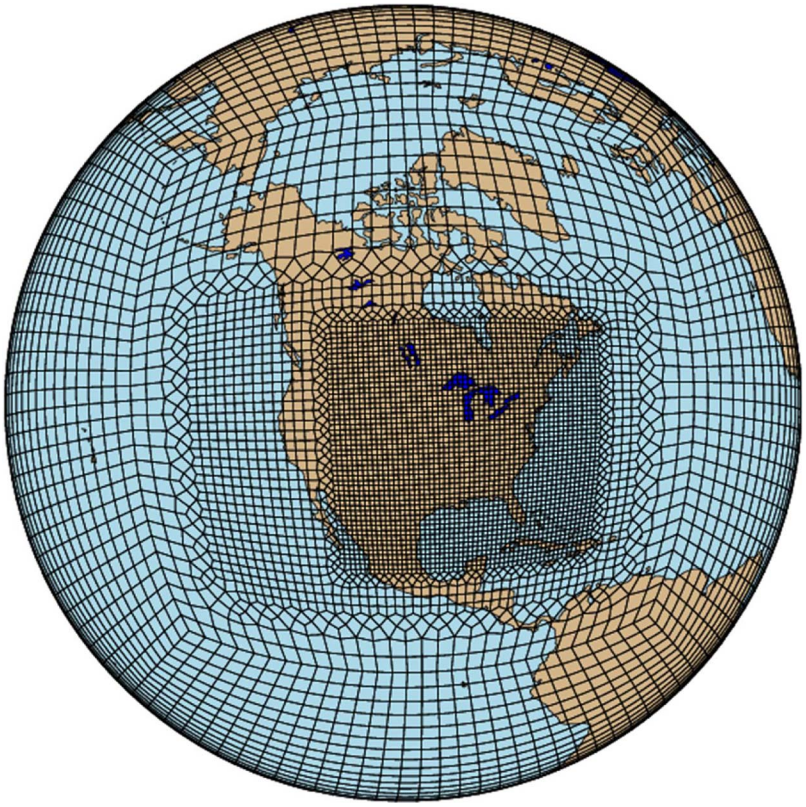

Fig. 2. Variable-Resolution Community Earth System Model (VR-CESM) model domains, including coarser 1° global grid and 0.25° refined mesh over the United States.

because each PFT within a given grid cell receives the same forcing meteorology from the CAM atmosphere.

The PFT-level output from VR-CESM and single point CLM (PTCLM), uniform PFT simulations driven by tower meteorology have been evaluated against the Duke and UNH eddy covariance tower data (Burakowski et al. in review). Comparisons between the towers and VR-CESM were very similar to uncoupled PTCLM simulation. It was found that during the growing season, modeled latent heat was biased low and sensible heat biased high over forests, which in turn affected simulation of the Bowen ratio. In winter, albedo persisted high over the UNH-grassland and UNH-cropland sites, and may be due to taller grass and weed canopy under the footprint of the net radiometer compared to the surrounding mowed and flattened field. Ongoing observational studies are evaluating the simulation of snowpacks at the UNH tower sites. Nonetheless, significant biases in VR-CESM are considered in the interpretation of the intrinsic biophysical results presented here.

2.3. Intrinsic Biophysical Mechanism (IBPM)

We apply the Intrinsic Biophysical Mechanism (IBPM) framework described in Lee et al. (2011) to the tower sites, PTCLM, and VR-CESM. The difference in surface temperature ($\Delta T_{s,calc}$) between an open field and reference forest site (open – forest) is calculated as the sum of the three terms representing the contribution of differences in albedo, energy redistribution due to differences in surface roughness, energy redistribution due to differences in the Bowen ratio, respectively:

$$\Delta T_{s,calc} = \frac{\lambda_0}{1+f}\Delta S + \frac{-\lambda_0}{(1+f)^2}R_n\Delta f_1 + \frac{-\lambda_0}{(1+f)^2}R_n\Delta f_2 \quad (1)$$

Where λ_0 is the temperature sensitivity resulting from the longwave radiation feedback ($=1/(4\sigma T_s^3)$, where $\sigma = 5.67 \times 10^{-8}$ W m^{-2} K^{-4}), ΔS is the difference in net shortwave radiation between open land and an adjacent reference forest site, f is the energy redistribution factor:

$$f = \frac{\rho C_p}{4 r_a \sigma T_{s,rad}^3}\left(1 + \frac{1}{\beta}\right) \quad (2)$$

where ρ is air density (= 1.225 kg m^{-3}), C_p is specific heat of air at constant pressure (1004.5 J kg^{-1} K^{-1}), r_a is the aerodynamic resistance. For the purposes of this study, r_a is calculated as follows:

$$r_a = \frac{\rho C_p (T_{s,rad} - \theta)}{H} \quad (3)$$

where θ is the potential air temperature and H is the sensible heat flux in W m^{-2}. We use θ in lieu of air temperature (T_a) to account for differences in measurement height for the different PFTs (Arya, 1988). Potential temperature (θ) is calculated as follows:

$$\theta = T_a\left(\frac{P_0}{P_{sfc}}\right)^{\frac{R}{C_p}} \quad (4)$$

Unrealistic values of r_a were removed. Specifically, when r_a was less than 0.001 s m^{-1}, which occurred when measured $T_s - \theta$ was opposite in sign to H, or when r_a was greater than 100 s m^{-1}, which occurred under very stable atmospheric boundary layer conditions. The observed and modeled β is calculated at hourly (eddy covariance and PTCLM4.5) and 3-hourly (VR-CESM1.3) intervals using the following equation:

$$\beta = \frac{\Sigma H}{\Sigma \lambda E} \quad (5)$$

where λE is the latent heat flux in W m^{-2}. $T_{s,rad}$ in Eqs. (2) and (3) is the radiative skin temperature of the reference forest, and β is the Bowen ratio of the reference forest. Radiative surface temperature ($T_{s,rad}$) used in Eqs. (2) and (3) was approximated using the Stefan-Boltzmann law,

$$T_{s,rad} = \sqrt[4]{\frac{LW_{out}}{\varepsilon\sigma}} \quad (6)$$

R_n is the net radiation in W m^{-2}, and Δf_1, and Δf_2 are the differences in energy redistribution due to surface roughness and Bowen ration, respectively:

$$\Delta f_1 = -f\frac{\Delta r_a}{r_a} \quad (7)$$

$$\Delta f_2 = -f\frac{\Delta \beta}{\beta^2} \quad (8)$$

where LW_{out} is the outgoing longwave radiation (W m^{-2}), ε is emissivity (=0.98).

We used Eq. (2) to solve $\Delta T_{s,calc}$ for each hourly time step in the eddy covariance tower observations and for each 3-hourly time step in VR-CESM. The calculated sum ($\Delta T_{s,calc}$, equation 1) of the intrinsic biophysical factors was compared to the difference in radiative temperature ($\Delta T_{s,rad}$) and to the difference in potential temperature ($\Delta\theta$) between forested (θ_{forest}) and open (θ_{open}) sites:

$$\Delta\theta = \theta_{open} - \theta_{forest} \quad (9)$$

3. Results

3.1. Diurnal patterns in biophysical factors influencing surface temperature

Analysis of the intrinsic biophysical factors at the tower sites and in VR-CESM reveals surface roughness as the dominant biophysical forcing factor that drives annual surface and potential air temperature differences between forested and open sites. Let us first consider the differences in annual surface temperature between hardwood forest and grassland, two land cover type pairs represented at the UNH cluster (Fig. 3a–f; left column) and at the Duke cluster (Fig. 3g–l; right column). At UNH, the individual biophysical contributions from differences in albedo (Fig. 3a), surface roughness (Fig. 3b), and Bowen ratio (Fig. 3c) indicated that surface temperature differences are due primarily to surface roughness differences, characterized by nighttime cooling and daytime warming over open lands compared to forested lands. This is true for the entire diurnal cycle in both models and observations, however the magnitude of daytime warming in $\Delta T_{s,calc}$ is considerably more than $\Delta T_{s,rad}$ and $\Delta\theta$ (Fig. 3d–f).

A similar diurnal pattern is observed when comparing Duke-hardwood and Duke-grass, with surface roughness dominating the sum of the components (Fig. 3j), the difference in radiative surface temperature ($T_{s,rad}$) as calculated from Eq. (6) (Fig. 3k), and the difference in potential temperature (Fig. 3l). Error bars (± 1 σ) are considerable for the sum of the components (Fig. 3j). Surface roughness also dominates the diurnal pattern in $\Delta T_{s,calc}$, $\Delta T_{s,rad}$, and $\Delta\theta$ at the other site-pair combinations (e.g., Duke-Pine vs. Duke-grass, Figs. S3; UNH-hardwood vs. UNH-crop, Fig. S4).

At both Duke and UNH, the diurnal surface roughness pattern indicates cooler temperatures over the grasslands at night compared to the adjacent forest, and warmer grassland temperatures during the day compared to hardwood forest. The magnitude of the nighttime cooling is generally captured well in VR-CESM for the sum of the biophysical components at UNH (Fig. 3d) and Duke (Fig. 3j). During the day, warmer grasslands are simulated by VR-CESM at UNH (Fig. 3d), but the magnitude is nearly half that observed in the towers at mid-day for the individual contribution of surface roughness (Fig. 3b), a signal that propagates into the sum of the components (Fig. 3d). The magnitude of nighttime cooling and daytime warming in the radiative surface temperature is also halved in VR-CESM compared to tower observations at UNH (Fig. 3e) and Duke (Fig. 3k). This means that VR-CESM tends to underestimate the contribution of surface roughness on surface temperature relative to observations.

Differences in surface temperature due to the albedo component are weak during the day in winter and negligible in the summer at all paired sites (Figs. S1; S3–S4). Energy redistribution due to differences in Bowen ratio has no significant impact on observed or modeled surface and potential air temperature differences in either winter or summer (Figs. S2–S4). The under prediction of latent heat and over prediction of sensible heat over forests during the growing season identified in Burakowski et al. (in review) contributes to greater uncertainty in the contribution of Bowen ratio differences in the modeled VR-CESM results. Nonetheless, surface roughness differences emerge as a dominant influence in both the towers and the VR-CESM.

3.2. Regional differences in surface temperature simulated by VR-CESM

As with the individual tower cluster analysis, surface roughness emerged as a dominant contributor explaining differences in surface temperature for PFT-level analysis of biophysical factors. As noted earlier, we emphasize that the coupled model runs presented here do not simulate any changes in land cover (*i.e.* deforestation) but instead compare within-grid cell differences between forested and deforested PFTs. As such, we have eliminated any indirect effects from changes in atmospheric circulation that may result from deforestation or other changes in land use and land cover. The VR-CESM results discussed below focus on surface temperature differences between deciduous broadleaf temperate hardwood forest and grassland PFTs. Additional PFT comparisons between crop-broadleaf deciduous temperate forest (Figs. S5–S7) and between grass-needleleaf evergreen temperate forest (Figs. S8-S10) can be found in the Supplementary Information.

The sum of the individual biophysical factors (Fig. 4a) contributing to annual differences in surface temperature indicates a weak cooling over open lands from the albedo component (Fig. 4b), strong warming due to surface roughness (Fig. 4c) and regions of weak cooling and weak warming from the Bowen ratio of grasslands compared to forested regions (Fig. 4d). The radiative surface temperature difference (Fig. 4e, calculated using Eq. (6)) indicates weak cooling in the northern part of the domain, in contrast to the wide-spread warming calculated from the sum of the individual components (Fig. 4a).

In winter, the sum of the biophysical components results in cooler grasslands in the northern latitudes and warmer grasslands in the southern half of the eastern US based on the VR-CESM simulations. In the northern latitudes, snow cover over open lands results in albedo cooling in the model (Fig. 5b). In the Southeastern US, surface roughness leads to warming over snow-free open lands (Fig. 5c). Differences in wintertime Bowen ratio contribute to warmer grasslands in the mid-Atlantic region of the eastern seaboard and southern New England (Fig. 5d). The within-grid cell radiative surface temperature difference between grasslands and deciduous broadleaf forests (Fig. 5e) closely resembles the albedo pattern (Fig. 5b).

Summertime surface temperature differences were dominated by the surface roughness signal in VR-CESM (Fig. 6). The sum of the biophysical components indicates that grasslands are 0.4 °C to 1.2 °C warmer than deciduous broadleaf forests that receive the identical atmospheric forcing. Differences in the Bowen ratio contribute to slightly cooler grasslands (−0.2 °C to −0.8 °C), while the albedo component differences in surface temperature were less than −0.2 °C. Differences in radiative surface temperature were between 0 °C and 0.4 °C (Fig. 6e).

4. Discussion

We note two major discrepancies in observed and modeled surface temperature differences between forested and open lands: (1) surface temperature differences calculated from the sum of biophysical components ($\Delta T_{s,calc}$) were consistently greater than differences in surface radiative temperature ($\Delta T_{s,rad}$) and potential temperature ($\Delta\theta$) in both observations and in VR-CESM, and (2) observed daytime warming over open lands due to low surface roughness is considerably greater than modeled results.

We hypothesize that these discrepancies could stem from one of the critical assumptions in the IBPM framework – specifically that “the air temperature, T_a, is identical at a blending height z_b” (Lee et al., 2011). The blending height, z_b, is the height at which the influence of surface heterogeneity falls below a threshold and can be expressed as

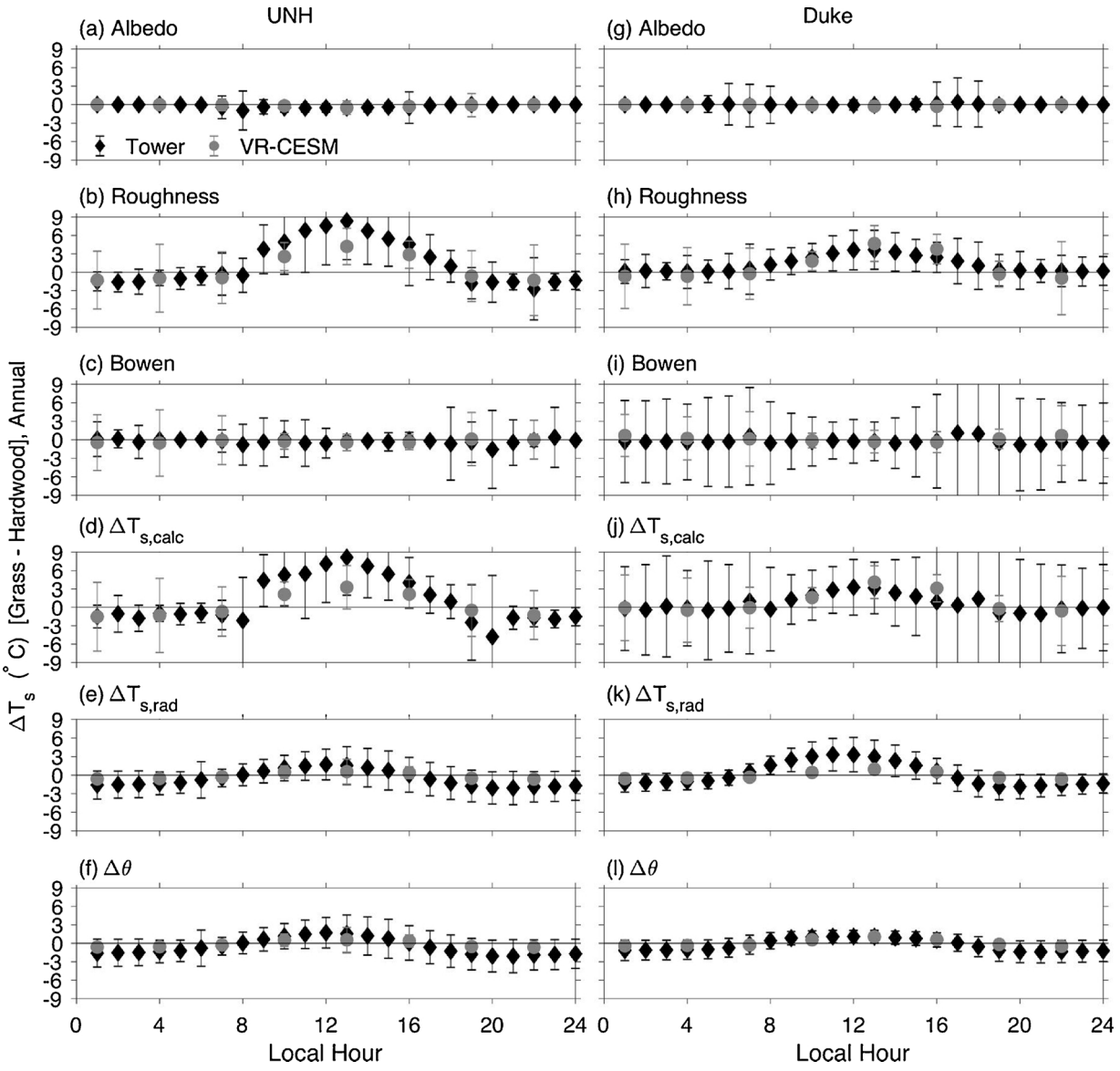

Fig. 3. Difference in annual surface temperature (ΔT_s) between UNH-grass and UNH- hardwood (a-f, left column) and between Duke-grass and Duke-hardwood (g-l, right column). Temperature differences shown due to individual Intrinsic Biophysical Mechanism components: albedo (a,g), roughness (b,h), Bowen ratio (c,i), as well as the calculated sum of the individual components from Eq. (1) (d,j; $\Delta T_{s,calc}$). The difference in radiative temperature from Eq. (6), (e,k; $\Delta T_{s,rad}$), and difference in potential temperature from Eqs. (4) and (9) (f,l; $\Delta\theta$) is also shown.

$$z_b = C\left(\frac{u^*}{U}\right)^p L_{hetero} \tag{10}$$

where u^* is the friction velocity based on the horizontally-averaged momentum flux, U is the speed of the spatially averaged wind vector based on the flow at blending height, L_{hetero} is the horizontal scale of the surface heterogeneity, p equals 2, and C is a nondimensional coefficient usually taken as unity (Mahrt 2000).

Typical eddy covariance tower observations provide measurements at fixed heights and cannot account for time-dependent shifts in the blending height. In the original Lee et al. (2011) IBPM framework, T_a over the forest may, under certain atmospheric states, be collected at a fixed height that approximates the blending height; however T_a at the open sites will almost always be measured below the blending height. The difference in measurement height could inflate ΔT_a, which manifests in potentially large variations in r_a (Eq. (4)) and further propagates into the energy redistribution term, f (Eq. (2)), the difference in energy redistribution due to surface roughness, Δf_1 (Eq. (7)), and the difference in energy redistribution due to Bowen ration, Δf_2 (Eq. (8)). Here, we used θ in lieu of T_a, but not that the $\Delta\theta$ is term is non-negligible and follows a non-uniform distribution at the UNH paired sites (Fig. 7a,b). At the Duke sites, the distribution is more uniform and centered around zero (Fig. 7c,d). Our use of θ in lieu of T_a attempted to account for differences in measurement height, however, the biases and distribution of $\Delta\theta$ are similar to ΔT_a at the UNH sites, meaning use of θ in lieu of T_a does not alleviate the measurement height vs. blending height assumption in IBPM. Accounting for the influence screen height on the IPBM blending height assumption should be a research priority in future studies.

Bright et al. (2017) note that f, the energy redistribution factor, tends to be greater over forest compared to fields, suggesting that forests are more efficient at dissipating latent and sensible heat through turbulent exchange during the day. We find similar results here with the emphasis on surface roughness dominating the difference in surface temperature between forests and fields, despite key differences in the calculation of f. In Bright et al. (2017), the energy redistribution term is calculated as follows:

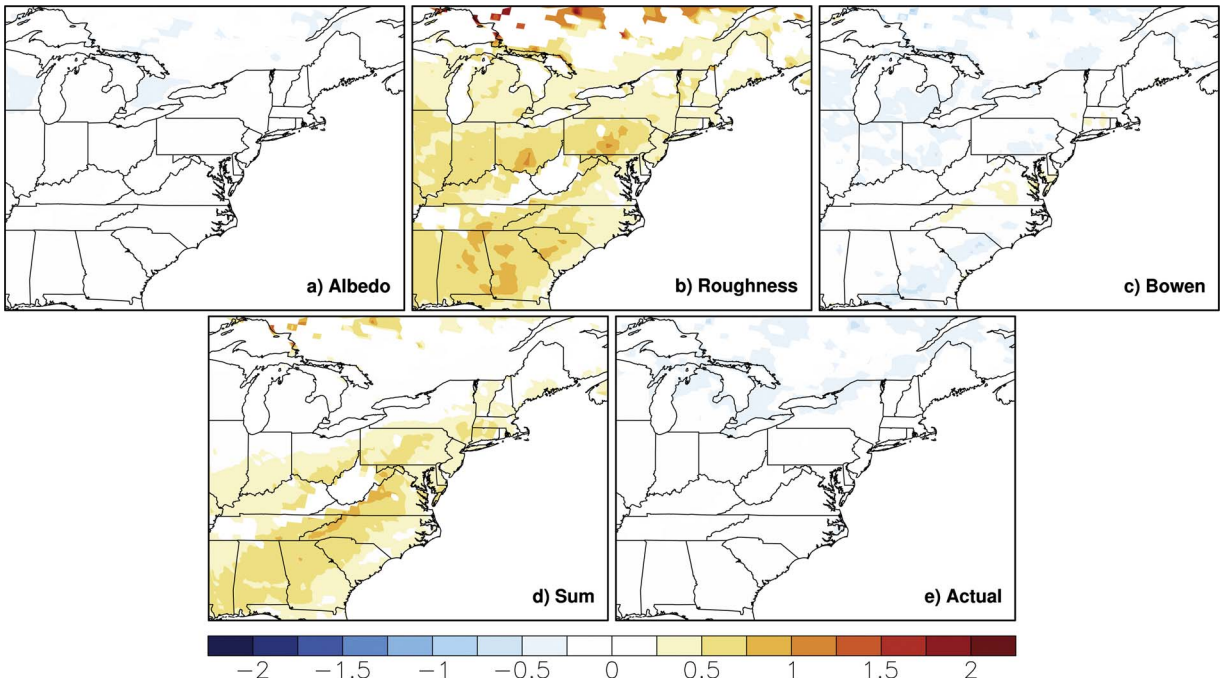

Fig. 4. Annual mean within-grid cell PFT difference (grass – broadleaf deciduous temperate forest) in surface temperature in VR-CESM1.3, showing the relative contributions of (a) albedo, (b) surface roughness, (c) Bowen ratio, and (d) the sum of the intrinsic biophysical factors. The (e) radiative surface temperature difference is calculated using Eq. (2). Warm colors indicate regions where open lands are warmer than forested lands; cool colors indicate areas where open lands are cooler than forested areas. Areas in grey indicate regions where broadleaf deciduous temperate forest and grass PFTs do not exist within the same grid cell.

$$f = \frac{\lambda_0}{T_s - T_a}(R_n^* - G) - 1 \quad (11)$$

where G is ground heat flux in W/m^2. The revised formulation of f removes r_a and β, and reduces uncertainty related to partitioning of turbulent fluxes (e.g., β) and energy budget closure. However, it does introduce uncertainty in G. At the Duke sites, measured G is a relatively small term (10–20 W/m^2), however G is biased high in VR-CESM, ranging from 100–150 W/m^2 in the Duke-grass simulation (Burakowski et al., *in review*). At the UNH sites, G was not measured and G in VR-CESM is of similar magnitude to the Duke sites. Given the strong bias in ground heat flux in the model and lack of G measurements at the UNH sites, we opted to use the original formulation of f (Eq. (2)) from Lee et al. (2011).

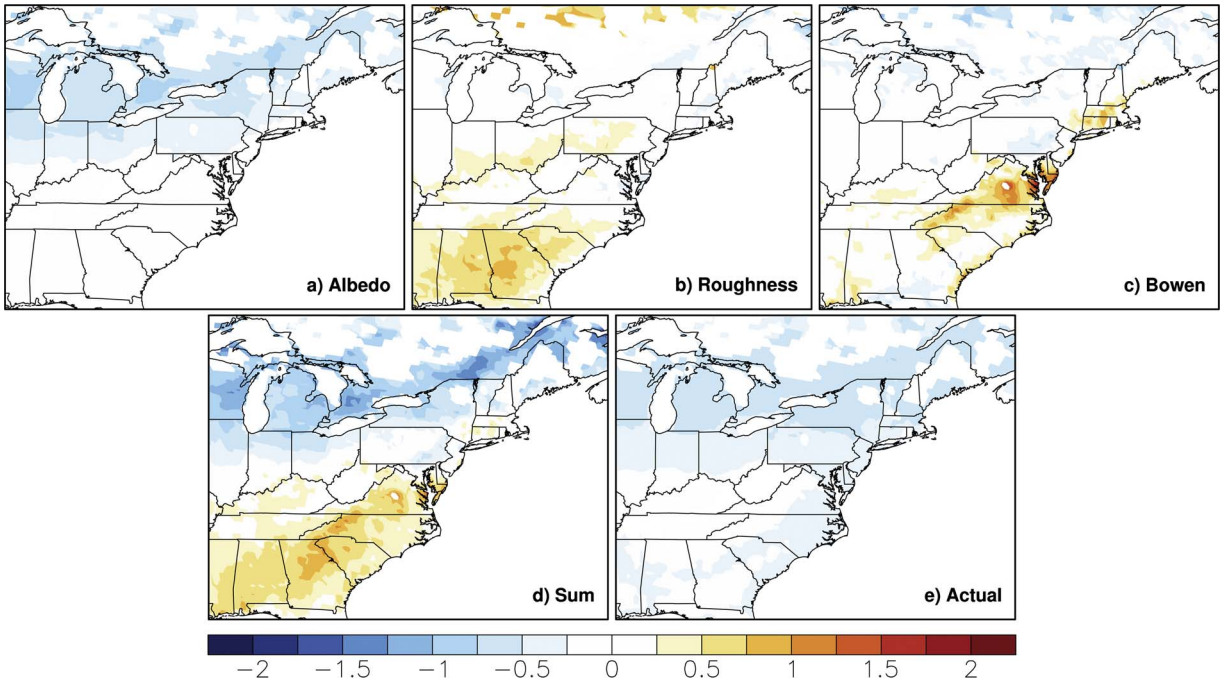

Fig. 5. Mean winter (December through February) within grid cell PFT difference (grass – broadleaf deciduous temperate forest) in surface temperature in VR-CESM1.3, showing the relative contributions of (a) albedo, (b) surface roughness, (c) Bowen ratio, and (d) the sum of the intrinsic biophysical factors. The (e) actual radiative surface temperature difference is calculated using Eq. (2). Warm colors indicate regions where open lands are warmer than forested lands; cool colors indicate areas where open lands are cooler than forested areas. Areas in grey indicate regions where broadleaf deciduous temperate forest and grass PFTs do not exist within the same grid cell.

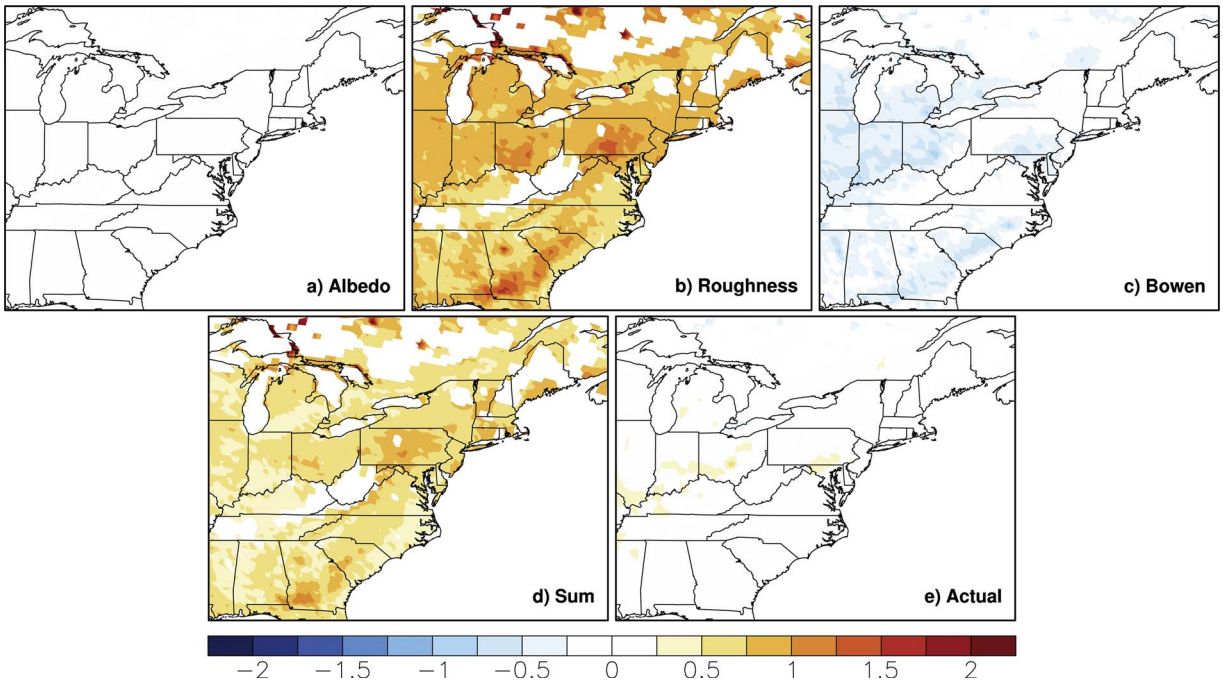

Fig. 6. Summer (June through August) mean within grid cell PFT difference (grass – broadleaf deciduous temperate forest) in surface temperature in VR-CESM1.3, the relative contributions of (a) albedo, (b) surface roughness, (c) Bowen ratio, and (d) the sum of the intrinsic biophysical factors. The (e) actual radiative surface temperature difference is calculated using Eq. (2). Warm colors indicate regions where open lands are warmer than forested lands; cool colors indicate areas where open lands are cooler than forested areas. Areas in grey indicate regions where broadleaf deciduous temperate forest and grass PFTs do not exist within the same grid cell.

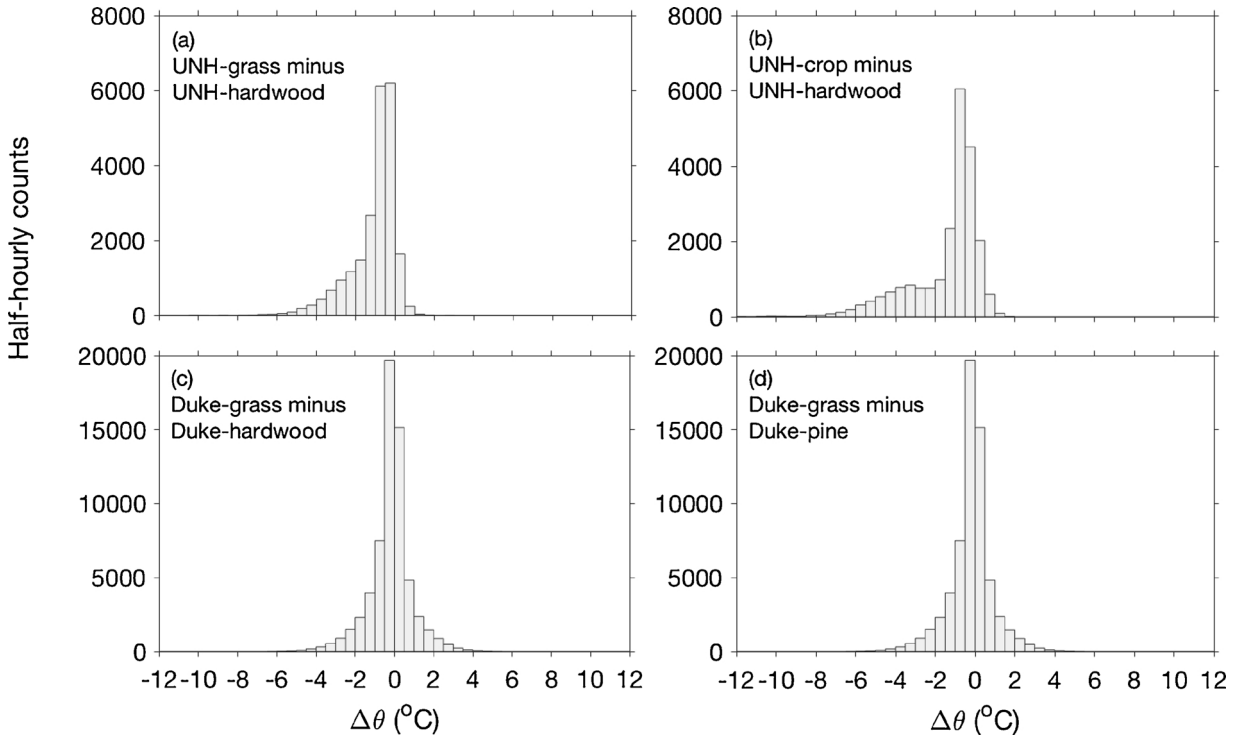

Fig. 7. Histograms of potential air temperature differences (open – forest; $\Delta\theta$) for the four site pairs: (a) UNH-grass minus UNH-hardwood, (b) UNH-crop minus UNH-hardwood, (c) Duke-grass minus Duke-hardwood, and (d) Duke-grass minus Duke-pine. $\Delta\theta$ is calculated using Eqs. (4) and (9).

The influence of surface heterogeneity within the grid cell resides in the 2 m air temperature variable, or TSA. TSA is the stability adjusted air temperature interpolated from the PFT-specific radiative surface temperature and the temperature from the lowest atmosphere model level, TBOT. In the model, TBOT is representative of the blending height and is identical for all PFTs within a given grid cell. The interpolated TSA is therefore representative of air temperature below the blending height, where the influence of surface heterogeneity is still apparent through its dependence on the PFT. A more appropriate analysis that meets the Lee et al. (2011) IBPM assumptions for T_a at the blending height, would be to use TBOT in lieu of TSA in the formulation for r_a, f, Δf_1, and Δf_2. However, 3-hourly averaged TBOT was not

available from the VR-CESM CAM output files.

The IBPM method assumes that surface temperature differences due to changes in albedo, surface roughness, and the Bowen ration are independent. However, Rigden and Li (2017) demonstrate that the assumption of independence is not complete and that the new two-resistance mechanism method they propose reduces the impact of surface roughness on temperature differences by 10–25% relative to the original IBPM method. We acknowledge that the methodology presented here likely overestimates the contribution of surface roughness by a similar magnitude. Nonetheless, surface roughness would remain the strongest contributor to daytime surface temperature differences.

Lack of energy budget closure at the Duke and UNH tower sites are another source of uncertainty in the IBPM results presented here. At Duke, energy budget imbalance is estimated to be around 20%. At UNH, the lack of G measurements precludes energy budget imbalance calculations, though we estimate it is similar to Duke and other FLUXNET sites (Wilson et al., 2002). In VR-CESM, the model forces energy budget closure but nonetheless exhibits underestimates latent heat and overestimates sensible heat over deciduous broadleaf and evergreen needleleaf temperate forests (Burakowski et al. *in review*).

Modeled biases in sensible and latent heat flux impact the modeled Bowen ratio (Burakowski et al. *in review*). A new canopy turbulence and roughness sublayer parameterization greatly improves latent and sensible heat fluxes for forested PFTs in CLM and maintains excellent agreement for short canopy PFTs (Bonan et al., in review). Given the insignificant contribution of Bowen ratio in the observed IBPM results reported here and in other studies (e.g., Bright et al., 2017; Chen and Dirmeyer, 2016; Lee et al., 2011) we do not expect significant changes in Bowen ratio contributions to $\Delta T_{s,calc}$. Nonetheless, it is important to consider model biases in surface energy fluxes when considering the impact of land cover on surface temperature.

5. Conclusions

The results presented here suggest that local surface temperature differences between forested and open lands in the eastern United States are strongly influenced by differences in surface roughness. Aerodynamically smoother open land canopies (e.g., grass, corn) are warmer during the day and cooler at night compared to aerodynamically rougher forest canopies. Differences in the Bowen ratio and albedo play a minor role on an annual basis. Albedo exerts a cooling influence during the winter for seasonally snow covered lands located in the northeastern US. These conclusions are supported by eddy covariance tower observations and by a Variable-Resolution coupled land atmosphere model. Uncertainties remain with respect to the magnitude of daytime warming due to surface roughness over open lands, which is overestimated using the intrinsic biophysical mechanism methodology presented in Lee et al. (2011) in comparison to modeled results and surface temperature differences calculated from radiative surface temperature and potential temperature.

We recommend that future research address the blending height assumptions in the IBPM framework, a task that is more easily addressed with sub-grid PFT-level model output than with observations. PFTs within the same grid-cell by definition receive the same atmospheric forcing from the lowest atmospheric model level. With observations, however, it is logistically challenging to collect hourly measurements of T_a at the blending height. Both eddy covariance systems and coupled land-atmosphere models have issues that make it challenging to definitively assign confidence in the IBPM results. For the VR-CESM model, biases in surface energy fluxes need to be resolved, while blending height assumptions and energy budget closure issues need to be addressed in eddy covariance systems. Nonetheless, surface roughness has emerged as exerting a dominant influence on surface temperature differences in the mid-latitudes due to land cover, both in this study and in others (Bright et al., 2017; Chen and Dirmeyer, 2016; Lee et al., 2011).

Acknowledgements

The authors acknowledge support of the National Science Foundation (grants EPS-1101245, EF-1048481 and EF-1638688), the NASA Terrestrial Ecology Program (NNX12AK56G S01), the New Hampshire Agricultural Experiment Station (USDA-NIFA #1006997), the Northern Ecosystems Research Cooperative (NERC). This study is a contribution of the NSF-supported Harvard Forest and Hubbard Brook Long-Term Ecological Research projects. We would also like to recognize the computational support provided by the NCAR Computational and Information Systems Laboratory for computing, processing, and data storage.

Appendix A. Supplementary data

Supplementary data associated with this article can be found, in the online version, at https://doi.org/10.1016/j.agrformet.2017.11.030.

References

Adegoke, J.O., Pielke Sr., R.A., Eastman, J., Mahmood, R., Hubbard, K.G., 2003. Impact of irrigation on midsummer surface fluxes and temperature under dry synoptic conditions: a regional atmospheric model study of the U.S. high plains. Mon. Weather Rev. 131, 556–564. http://dx.doi.org/10.1175/1520-0493(2003)131.

Arya, S.P., 1988. Introduction to Micrometeorology. Academic Press, San Diego.

Baldocchi, D., Ma, S., 2013. How will land use affect air temperature in the surface boundary layer? Lessons learned from a comparative study on the energy balance of an oak savanna and annual grassland in California, USA. Tellus B 65, 19994. http://dx.doi.org/10.3402/tellusb.v65i0.19994.

Betts, A.K., Ball, J.H., 1997. Albedo over the boreal forest. J. Geophys. Res. 10 (28) (901-28, 909).

Betts, R.A., Falloon, P.D., Klein Goldewijk, K., Ramankutty, N., 2007. Biogeophysical effects of land use on climate: model simulations of radiative forcing and large-scale temperature change. Agric. For. Meteorol. 142, 216–233.

Betts, R.A., 2001. Biogeophysical impacts of land use on present-day climate: near-surface temperature change and radiative forcing. Atmos. Sci. Lett. 1, 39–51. http://dx.doi.org/10.1006/asle.2001.0023.

Boisier, J.P., de Noblet-Ducoudré, N., Pitman, A.J., Cruz, F.T., Delire, C., van den Hurk, B.J.J.M., van der Molen, M.K., Müller, C., Voldoire, A., 2012. Attributing the impacts of land-cover changes in temperate regions on surface temperature and heat fluxes to specific causes: results from the first LUCID set of simulations. J. Geophys. Res. 117, D12116. http://dx.doi.org/10.1029/2011JD017106.

Bonan, G.B., Patton, E., Harman, I., Oleson, K., Finnigan, J., Lu, Y., Burakowski, E.A., Modeling canopy-induced turbulence in the Earth system: a unified parameterization of turbulent exchange within plant canopies and the roughness sublayer (CLM-ml v0). Geo. Sci. Mod. Dev. Disc. doi:10.5194/gmd-2017-261.

Bonan, G.B., 2008. Forests and climate change: forcings, feedbacks, and the climate benefits of forests. Science 320, 1444–1449. http://dx.doi.org/10.1126/science.1155121.

Bright, R.M., Davin, E., O'Halloran, T., Pongratz, J., Zhao, K., Cescatti, A., 2017. Local temperature response to land cover and management change driven by non-radiative processes. Nat. Clim. Change 7, 296–302. http://dx.doi.org/10.1038/nclimate3250.

Brovkin, V., Claussen, M., Driesschaert, E., Fichefet, T., Kicklighter, D., Loutre, M.F., Matthews, H.D., Ramankutty, N., Schaeffer, M., Sokolov, A., 2006. Biogeophysical effects of historical land cover changes simulated by six Earth system models of intermediate complexity. Clim. Dyn. 26, 587–600.

Burakowski, E.A., Ollinger, S.V., Bonan, G.B., Wake, C.P., Dibb, J.E., Hollinger, D.Y., 2016. Evaluating the climate effects of mid-1800s deforestation in New England USA, using a Weather, Research, and Forecasting (WRF) model multi-physics ensemble. J. Clim. 29, 5141–5156.

Burakowski, E.A., Tawfik, A.B., Ouimette, A., Lepine, L., Zarzycki, C., Novick, K.A., Ollinger, S.V., Bonan, G.B., Simulating surface energy fluxes using uncoupled and coupled Earth System Models and eddy covariance tower clusters. Theoretical and Applied Climatology, submitted per publication.

Chen, L., Dirmeyer, P.A., 2016. Adapting observationally based metrics of biogeophysical feedbacks from land cover/land use change to climate modeling. Environ. Res. Lett. 11. http://dx.doi.org/10.1088/1748-9326/11/3/034002.

Davin, E.L., de Noblet-Ducoudré, N., 2010. Climate impact of global-scale deforestation: radiative versus non-radiative processes. J. Clim. 23, 97–112.

Davin, E.L., de Noblet-Ducoudré, N., Friedlingstein, P., 2007. Impact of land cover change on surface climate: relevance of the radiative forcing concept. Geophys. Res. Lett. 34, L13702. http://dx.doi.org/10.1029/2007GL02678.

de Noblet-Ducoudré, N., Boisier, J.-P., Pitman, A., Bonan, G.B., Brovkin, V., Cruz, F., Delire, C., Gayler, V., van den Hurk, B.J.J.M., Lawrence, P.J., van der Molen, M.K., Müller, C., Reick, C.H., Strengers, B.J., Voldoire, A., 2012. Determining Robust Impacts of Land-Use-Induced Land Cover Changs on Surface Climate over North America and Eurasia: Results from the First Set of LUCID Experiments. J. Clim. 25, 3261–3281.

Feddema, J.J., Oleson, K.W., Bonan, G.B., Mearns, L.O., Buja, L.E., Meehl, G.A., Washington, W.M., 2005. The importance of land-cover change in simulating future

climates. Science 310, 1674–1678. http://dx.doi.org/10.1126/science.1118160.
Gates, L., 1992. AMIP: the atmospheric model intercomparison project. Bull. Am. Meteorol. Soc. 73, 1962–1970.
Jin, Y., Schaaf, C.B., Gao, F., Li, X., Strahler, A., Zeng, X., Dickinson, R.E., 2002. How does snow impact the albedo of vegetated surfaces as analyzed with MODIS data? Geophys. Res. Lett. 29 (10), 1374. http://dx.doi.org/10.1029/2001GL014132.
Juang, J.-Y., Katul, G., Siqueira, M., Stoy, P., Novick, K., 2007. Separating the effects of albedo from eco-physiological changes on surface temperature along a successional chronosequence in the southeastern United States. Geophys. Res. Lett. 34, L21408. http://dx.doi.org/10.1029/2007.GL031296.
Kueppers, L.M., Snyder, M.A., Sloan, L.C., 2007. Irrigation cooling effect: regional climate forcing by land-use change. Geophys. Res. Lett. 34, L03703. http://dx.doi.org/10.1029/2006GL028679.
Kvalevåg, M.M., Myhre, G., Bonan, G., Levis, S., 2010. Anthropogenic land cover changes in a GCM with surface albedo changes based on MODIS data. Int. J. Climatol. 30, 2105–2117. http://dx.doi.org/10.1002/joc.2012.
Lawrence, P.J., Chase, T.N., 2010. Investigating the climate impacts of global land cover change in the community climate system model. Int. J. Climatol. 30, 2066–2087. http://dx.doi.org/10.1002/joc.2061.
Lee, X., et al., 2011. Observed increase in local cooling effect of deforestation at higher latitudes. Nature 479, 384–387. http://dx.doi.org/10.1038/nature10588.
Li, Y., Zhao, M., Motesharrei, S., Mu, Q., Kalnay, E., Li, S., 2015. Local cooling and warming effects of forests based on satellite observations. Nat. Commun. 6. http://dx.doi.org/10.1038/ncomms7603.
Luyssaert, S., et al., 2014. Land management and land-cover change have impacts of similar magnitude on surface temperature. Nat. Clim. Change 4, 389–393. http://dx.doi.org/10.1038/nclimate2196.
Mahrt, L., 2000. Surface heterogeneity and vertical structure of the boundary layer. Bound. Layer Meteorol. 96, 33–62.
Moody, E.G., King, M.D., Schaaf, C.B., Hall, D.K., Platnick, S., 2007. Northern Hemisphere five-year average (2000–2004) spectral albedos of surfaces in the presence of snow: statistics computed from Terra MODIS land products. Remote Sens. Environ. 111, 337–345.
Neale, R.B., et al., 2010. Description of the NCAR Community Atmosphere Model (CAM5.0). NCAR Tech. Note NCAR/TN-4861STR. (268 pp. Available online at www.cesm.ucar.edu/models/cesm1.1/cam/docs/description/cam5_desc.pdf).
Novick, K.A., Oren, R., Stoy, P.C., Siqueira, M.S., Katul, G., 2009. Nocturnal evapotranspiration in eddy covariance records from three co-located ecosystems in the Southeastern US: the effect of gapfilling methods on estimates of annual fluxes. Agric. For. Meteorol. 149, 1491–1504. http://dx.doi.org/10.1016/j.agrformet.2009.04.005.
Novick, K.A., Oishi, A.C., Ward, E.J., Siqueira, M.B.S., Juang, J.-Y., Stoy, P.C., 2015. On the difference in the net ecosystem exchange of CO_2 between deciduous and evergreen forests in the southeastern United States. Global Change Biol. 21, 827–842. http://dx.doi.org/10.1111/gcb.12723.
Oleson, K.A., et al., 2013. Technical Description of version 4.5 of the Community Land Model (CLM). NCAR/TN-503+STR. Available at: http://www.cesm.ucar.edu/models/cesm1.2/clm/CLM45_Tech_Note.pdf (last access: 28 December 2015).
Rigden, A.R., Li, D., 2017. Attribution of surface temperature anomalies induced by land use and land cover changes. Geophys. Res. Lett. 14. http://dx.doi.org/10.1002/2017GL073811.
Rotenberg, E., Yakir, D., 2010. Contribution of semi-arid forests to the climate system. Science 327, 451–454.
Schultz, N.M., Lawrence, P.J., Lee, X., 2017. Global satellite data highlights the diurnal asymmetry of the surface temperature response to deforestation. J. Geophys. Res. 122. http://dx.doi.org/10.1002/2016JG003653.
Wilson, K., Goldstein, A., Falge, E., Aubinet, M., et al., 2002. Energy balance closure at FLUXNET sites. Agric. For. Meteorol. 113, 223–243.
Zarzycki, C.M., Levy, M.N., Jablonowski, C., Overfelt, J.R., Taylor, M.A., Ullrich, P.A., 2014. Aquaplanet experiments using CAM's variable-resolution dynamical core. J. Clim. 27, 5481–5503. http://dx.doi.org/10.1175/JCLI-D-14-00004.1.
Zarzycki, C.M., Jablonowski, C., Thatcher, D.R., Taylor, M.A., 2015. Effects of localized grid refinement on the general circulation and climatology in the community atmosphere model. J. Clim. 28, 2777–2803. http://dx.doi.org/10.1175/JCLI-D-14-00599.1.
Zhao, K., Jackson, R.B., 2014. Biophysical forcings of land-use changes from potential forestry activities in North America. Ecol. Monogr. 84, 329–353.